Journal of The Electrochemical Society, 2021 **168** 090502

Operando Measurements of Electrolyte Li-ion Concentration during fast charging with FTIR/ATR

Lydia Meyer,[1,*,z] David Curran,[1,] Ryan Brow,[2] Shriram Santhanagopalan,[2,**] and Jason Porter[1,z]**

[1]*Colorado School of Mines, Golden, Colorado 80401, United States of America*
[2]*National Renewable Energy Laboratory, Golden, Colorado, United States of America*

The ability to charge a Li-ion battery at high charging rates is critical for electric vehicle adoption; however, further study of ion transport is required to develop electrolytes suitable for fast charge. Fourier transform infrared spectroscopy (FTIR) used with attenuated total reflection (ATR) enables operando measurements of liquid electrolytes. This research focused on solvation shifting of solvent infrared absorption bands in the presence of lithium ions. Lithium-shifted infrared absorption bands and non-shifted bands of ethyl methyl carbonate (EMC) and ethylene carbonate (EC) were compared to infer ion concentration changes during cycling. Lithium concentrations were calibrated using EC/EMC/$LiPF_6$ electrolytes with known lithium concentrations. A Li-ion half-cell with a graphite anode and EC/EMC/$LiPF_6$ electrolyte was observed with FTIR/ATR. The results showed that the magnitude of lithium concentration changes increased with increasing C-rate. During a galvanostatic intermittent titration technique (GITT) test, changes in lithium concentration could be observed. During intercalation, a lithium depletion occurred when a negative current was applied, and a lithium surplus occurred during deintercalation when a positive current was applied. The capability of observing lithium concentration has significant implications for the utility of operando studies and the potential to link lithium movement to battery performance.
 [DOI: 10.1149/1945-7111/ac1d7a]

Manuscript submitted June 2, 2021; revised manuscript received July 26, 2021. Published September 6, 2021. *This was Paper 634 presented during PRiME 2020, October 4–9, 2020.*

From thermal safety to cycling stability, Li-ion batteries have advanced significantly in recent decades.[1,2] To reach the next level of battery innovation, however, new diagnostic approaches must be successfully demonstrated and utilized to address current Li-ion battery shortcomings that impede technological progress. Such shortcomings include the performance issues that occur during fast charging (2–10 C). Fast charging is associated with several safety and performance issues, such as thermal runaway, reduced charge capacity, reduced lifetimes, and charge degradation, which is the capacity reduction of a cell due to fluctuations in state-of-charge.[3–5] Improving the performance and safety of fast charging is critical for electric vehicle (EV) charging in approximately the same amount of time required to refuel an internal combustion engine vehicle.[6] While fast charging requires innovations in electrodes, electrolytes, and battery management systems, researchers are increasingly focused on developing electrolytes with sufficient ionic transport, electrochemical stability, and thermal stability for fast charging. Solid electrolytes offer improved thermal stability, but their ionic conductivity remains too low for fast charging ($\kappa_{solid} \approx 10^{-3}$ S cm^{-1} vs $\kappa_{liquid} \approx 10^{-2}$ S cm^{-1}).[7] Traditional organic electrolytes used in almost all commercial Li-ion batteries, while having high ionic conductivity, suffer from low transference number, ($t^+ = 0.3$–0.4), poor thermal stability, and are unsuitable against high-voltage electrodes. When used in fast-charging conditions, large ionic concentration gradients occur through the electrode thickness, thereby reducing charge capacity.[7] This is especially problematic for the electrodes proposed for EV batteries.

Improved in situ diagnostic tools are needed to gain greater insight into fundamental transport and electrochemical mechanisms in batteries, allowing researchers to select more promising battery materials and architectures.[8] In situ optical diagnostics, especially Fourier transform infrared spectroscopy (FTIR) coupled with attenuated total reflection (ATR), have shown promise in analyzing the performance of battery electrolytes under thermal abuse and in novel electrode chemistries.[9–16] In situ studies with FTIR have also investigated the effects of chemical additives and the solid electrolyte interface (SEI) layer growth on battery performance, as well as lithium plating, lithium intercalation, solvation processes, and other electrochemical reactions.[16,17] The absorption bands in infrared (IR) spectra correspond to specific vibrational modes of molecules, including those used in current Li-ion batteries: ethylene carbonate (EC), ethyl methyl carbonate (EMC), and lithium hexafluorophosphate ($LiPF_6$).[18] Measuring the IR spectra of liquid electrolytes in an operating battery enables correlation between absorption features and the concentration of electrolyte species, including solvents, salts, and additives. Many research questions surrounding this area of in situ optical diagnostics used to study Li-ion batteries remain unexplored.

Operando IR spectroscopy, in situ measurements of an operating battery, can be utilized to observe novel battery chemistries in real time and discover new promising electrolytes, as well as the electrochemical properties that enable fast charging. *En route* to that capability is the validation and further development of in situ IR diagnostics to observe proven battery chemistries. In this research, transport processes were observed with FTIR/ATR, including solvation shifting of lithium ions in liquid electrolytes at various charging rates. Solvation shifting occurs when electrolyte molecules form a shell-like structure around ions in the electrolyte because of charge attraction. Ionic attraction between ions and solvent molecules slightly alters select vibrational modes in the electrolyte molecule, causing the shifting of absorption bands in IR spectra. The resulting IR spectral changes can be correlated with ion concentration.

Density functional theory (DFT) has been used to investigate interactions between solvents and ions, and some researchers have specifically examined solvation in Li-ion cells with DFT. Chen et al. analyzed interactions between cations, anions, and solvents in electrolyte under vacuum conditions to investigate the dissolution behavior of lithium salt in electrolyte.[19] Borodin et al. used Born-Oppenheimer molecular dynamics to study the composition of the lithium solvation shell in various types of carbonate-based electrolytes and determined coordination preferences of lithium cations at different salt concentrations. Borodins results were validated with results from previous Raman and IR experiments.[20] Many researchers have observed solvation shifting experimentally. Xu used impedance analyses to study the charge-transfer process at the interface between the graphite anode and electrolyte to determine process activation energies. From this analysis, Xu determined that the Li^+ solvation structure depends on the type of carbonate

*Electrochemical Society Student Member.
**Electrochemical Society Member.
[z]E-mail: lydiameyer@mines.edu; jporter@mines.edu

molecules present in the electrolyte.[21] In a related study, Xu used nuclear magnetic resonance (NMR) to study the surface chemistries of the graphite/electrolyte interface and Li^+ solvation at low temperatures.[22] Yang et al. also used NMR spectroscopy to study Li^+ coordination with different carbonate molecules and determined that EC binds lithium ions more strongly, compared to dimethyl carbonate (DMC) and diethyl carbonate (DEC).[23] Matsubara et al. utilized NMR spectroscopy to study six different solvent systems and determined the Li^+ coordination shift that occurred for each solvent system and thus characterized the coordinating ability for each solvent system.[24] NMR has also been used in operando studies of lithium concentration in Li-ion batteries, a research pursuit similar to what is reported here. Krachhovskiy et al. used NMR to determine a detailed profile of an ionic species in a solution yielding the salt diffusivity and transference number of lithium ions in a Li-ion battery.[25] In a later study, they analyzed the spatial and temporal distribution of lithium in a cycling Li-ion battery. They also discovered a charging profile more conducive for the complete lithiation of a thick graphite electrode, which could be used in an EV battery.[26] While NMR is an attractive technique for studying the lithiation of graphite electrodes, FTIR/ATR offers much faster measurements, which will be valuable for studying fast charging. In another study with a non-linear spectroscopic technique, Tanim et al. used X-ray diffraction to study irreversible lithium plating under fast-charge conditions and found that the amount of lithium plating contributes directly to the amount of capacity fade in the cell.[27]

Fulfer and Kuroda conducted research on solvation shifting of lithium ions in different organic electrolytes with FTIR/ATR. Using an optical cell, they studied the structure and dynamics of DMC, EMC, and DEC with $LiPF_6$ and found that the linear carbonates form tetrahedral solvation cells around lithium ions.[28] In an earlier IR study, Fulfer and Kuroda also found that butylene carbonate and DMC form tetrahedral solvation shells and confirmed this finding with ab initio frequency calculation methods.[29] Related research has been conducted on quantifying lithium concentration. Yamanaka et al. used ultrafine Raman probes at different positions in a Li-ion battery to determine the change in lithium concentration during cycling.[30] Using FTIR/ATR, Marino et al. observed lithium concentration in a conversion electrode.[31] In a study combining techniques, Ellis et al. also used FTIR, as well as machine learning techniques, to determine $LiPF_6$ concentrations and compared the results with gas chromatography and inductively coupled plasma optical emission spectrometry methods.[32] Lastly, Paul et. al reviewed various techniques used to study lithium concentration and dynamics in Li-ion batteries, including several operando spectroscopy techniques, such as NMR and electron paramagnetic resonance spectroscopy.[33]

Here we report a novel quantitative infrared diagnostic for operando lithium ion concentration measurements under fast-charge conditions. In this research, we assembled a Li-ion half-cell and cycled it at various C-rates while collecting FTIR spectra. Using calibration data, we then calculated lithium concentration in the graphite anode during cycling. This research experimentally verified lithium concentration polarization profiles modeled by Diedrichson et al.[7] and Colclasure et al.[34] Research by Diedrichson et al. and Colclasure et al. was monumental for showing lithium concentration polarization associated with faster C-rates, and continued study of this phenomenon is critical for Li-ion battery development for EV applications.

Methods

Li-ion cell assembly and experimental setup.—The Li-ion battery half-cell utilized in the experiments for this study is depicted in Fig. 1. A modified 2032 coin cell was assembled on a diamond ATR plate in a glove box filled with argon gas. A copper current collector with a center hole (diameter = 1.6 mm) was placed on the ATR plate enabling optical access to the graphite electrode of the half-cell. The composition of the electrode was 91% graphite, 4.5% conductive carbon, and 4.5% PVDF binder by weight, and the electrode was prepared by tape casting directly onto a Celgard separator. The electrolyte for the battery tests was prepared in an argon-filled glove box with 1.2M $LiPF_6$ in EC/EMC = 50/50 (vol./vol., battery grade, Sigma-Aldrich). The graphite electrode, which had been soaked in electrolyte for at least 30 minutes, was placed anode-side down on the 75 μm thick copper foil. A 25 μm Celgard separator (diameter = 15 mm) was placed on top of the electrode/separator (thickness = 20 μm/25 μm). Lithium foil (ribbon, 0.38 mm × 23 mm, Sigma-Aldrich), calandered to a thickness of 150 μm, was placed on top of the separator. Stainless steel spreader plates (diameter = 15.5 mm) and a stainless steel wave spring (diameter = 14.5 mm) separated the lithium foil from the 2032 can. The ATR plate with the assembled half-cell was then removed from the glove box and reattached to the FTIR. The FTIR used in this research was the Nicolet iS50 (Thermo Fisher Scientific) with a deuterated triglycine sulfate (DTGS) detector, a resolution of 4 cm^{-1}, and a 10-scan average for battery tests. Before any tests were performed, the half-cell underwent two formation cycles at 50 μA (0.1 V to 1.5 V). The battery capacity for this cell was 0.3 mAh.

Electrochemical testing and validation.—A current dwell test was performed on the half-cell. The battery was cycled using an EZstat Pro potentiostat/galvanostat. The experiment followed a similar procedure to the galvanostatic intermittent titration technique (GITT) described by Verma et al.[35] The half-cell was tested with a GITT-like procedure at charging rates (anode intercalation) of 300 μA and 900 μA and discharging rates (anode deintercalation) of 700 μA. The FTIR was operated at a 10-scan average, so the device collected a spectrum approximately every 25 s. The pulse width for the GITT experiments was selected so that several FTIR data points could be collected during each dwell.

EC/EMC/$LiPF_6$ molarities test.—Electrolytes were prepared in an argon-filled glove box in quantities of 5 ml with $LiPF_6$ molarities of 0.5 mol l^{-1}, 0.75 mol l^{-1}, 1 mol l^{-1}, 1.25 mol l^{-1}, and 1.5 mol l^{-1}. These electrolytes were flushed through a flow cell mounted to the ATR, and absorption spectra were collected at a 32-scan average with a resolution of 4 cm^{-1}. The resulting spectra were analyzed to find solvation-shifting relationships associated with vibrational modes of EC and EMC. No current was applied through the solution during the calibration runs.

Results

The spectra collected during the EC/ EMC/$LiPF_6$ molarities test contain several lithium-shifted vibrational bands associated with EC and EMC. Table I summarizes the lithium-shifted bands and non-lithium-shifted bands observable in the IR spectra. As the electrolyte molarity was increased during the experiment, the number of solvent molecules coordinating with ions also increased, resulting in increased absorption for lithium-shifted vibrational bands. Figure 2

Table I. Lithium-shifted and non-lithium-shifted vibrational bands of EC/EMC/$LiPF_6$ electrolyte.

Wavenumbers[a] (cm^{-1})	Vibrational Mode
557	$LiPF_6$[36]
716, 728	EC ring bending[37]
838	PF_6^-[38]
1071, 1085	EC O-C-O asymmetric stretch[39]
1158, 1196	EC CH_2 twist[37]
1260, 1300	EMC O-C-O asymmetric stretch[40]
1742, 1712	EMC C=O[28]

a) (non-lithium shifted), (lithium shifted).

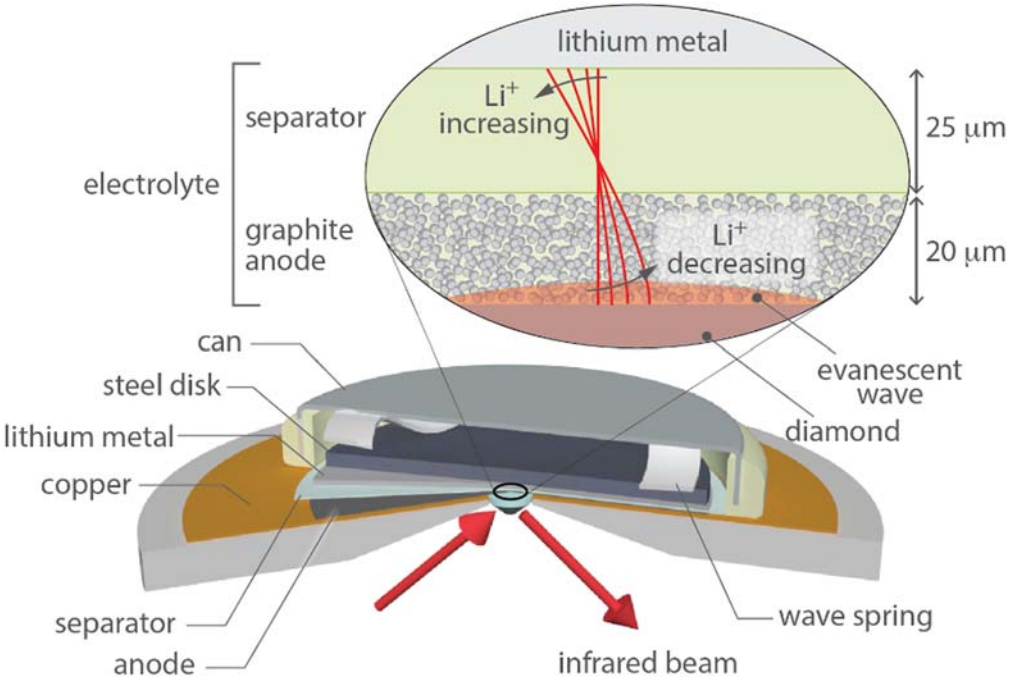

Figure 1. Optically accessible Li-ion half-cell. Inset shows lithium concentration profiles during charge.

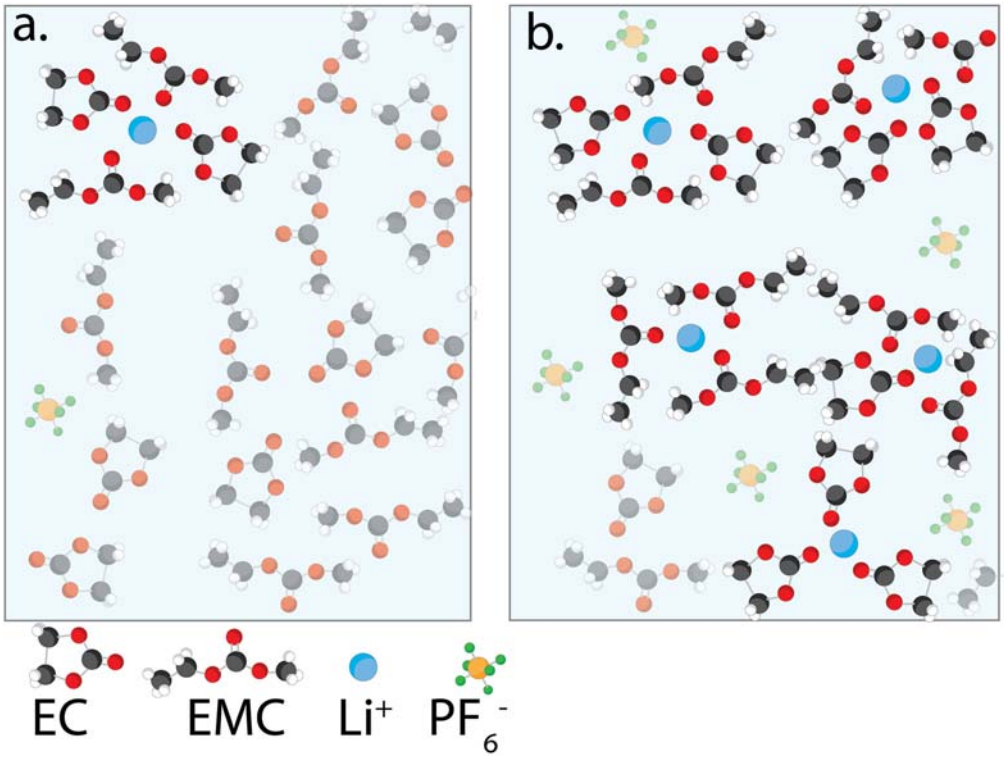

Figure 2. (a) Fewer lithium ions in the electrolyte leads to fewer electrolyte molecules forming solvation shells, compared to (b) in which a higher concentration of lithium ions induces the formation of more solvation shells.

shows the formation of solvation shells by EC and EMC molecules, which then induces changes in IR absorption bands. As more solvent molecules coordinate with lithium ions, the lithium-shifted IR bands will increase in absorbance relative to the non-lithium-shifted IR bands. Increasing Li^+ concentration simultaneously resulted in decreasing absorption for vibrational bands of uncoordinated solvent molecules. Figure 3 shows the results of the EC/EMC/$LiPF_6$ molarities test. The relative change in absorbance of lithium-shifted and non-lithium-shifted bands was used to infer lithium concentration.

Two pairs of IR bands, representing two separate solvated and non-solvated vibrational modes, were analyzed to determine linearity of the band absorption ratio with the molarity of $LiPF_6$ in the electrolyte. The bands with wavenumbers 1260 cm^{-1} and

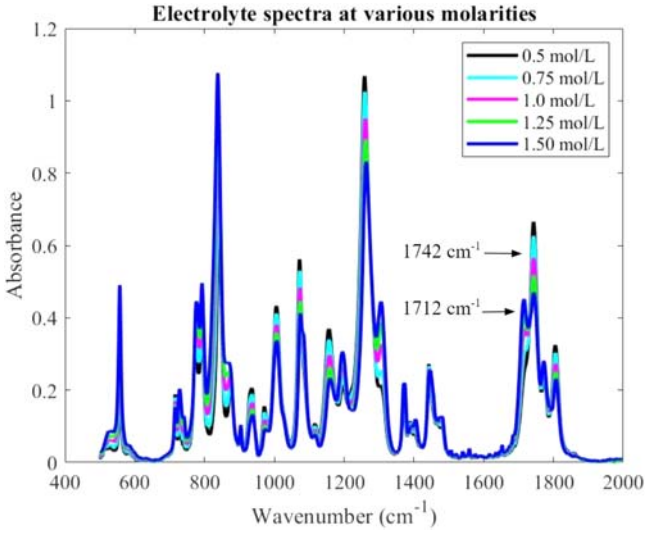

Figure 3. Infrared spectra of EC/EMC/$LiPF_6$ electrolyte in liquid cell on FTIR/ATR at various $LiPF_6$ molarities.

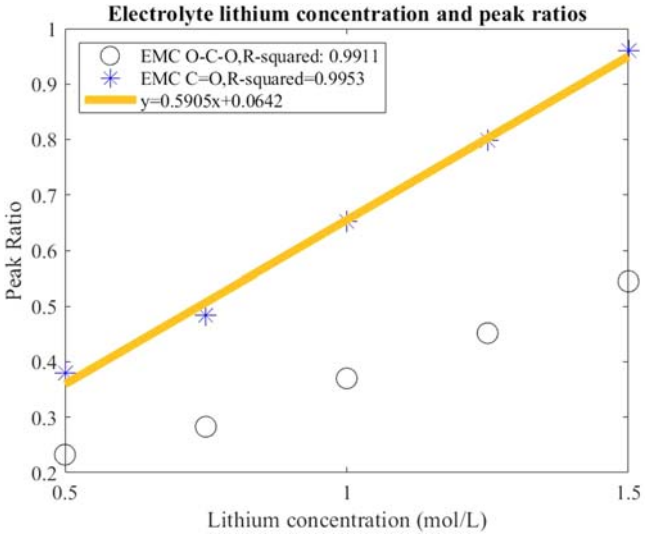

Figure 4. Relationship of molarity and Li-shift ratio.

1300 cm^{-1} are associated with the EMC oxygen-carbon-oxygen single-bond structure.[37] The bands at wavenumbers 1712 cm^{-1} and 1742 cm^{-1} are associated with the vibrational mode of EMC carbon-oxygen double bond.[24] The two vibrational mode pairs had strong linear correlations between electrolyte molarity and ratio of the Li-shifted band to the non-Li-shifted band (Fig. 4).

The absorbance ratio is defined as the ratio of the absorption band height of Li-shifted EMC C=O (1712 cm^{-1}) to the height of the non-Li-shifted EMC C=O absorption band (1742 cm^{-1}). The band height value was taken from the maximum of the absorption feature. This ratio was ultimately selected to determine lithium ion concentration in the bulk electrolyte at the back of the anode due to strong IR absorption and because the relationship between molarity and the absorbance ratio was highly linear. Additionally, according to the literature, the carbonyl bands of EMC tend to be excitonic and wrap around a nearby lithium ion, causing shifts in the IR band of the molecule, which further supports the use of the carbonyl band as a proxy for lithium concentration in the electrolyte.[28] Using the MATLAB Curve Fitting tool, the relationship between molarity and lithium ion concentration at the back of the anode was determined to be

$$x = (y - 0.0642)/0.5905 \quad [1]$$

where y is the ratio and x is the $LiPF_6$ molarity in the electrolyte in mol l^{-1}. Equation 1 was then used to determine the lithium concentration in a battery from the IR spectrum using the ratio of the absorbances of EMC IR bands. The root mean square error of the absorbance ratio in the liquid-only measurement from the relationship determined in Eq. 1 was 0.02 mol l^{-1}. This value represents the absolute accuracy of the method. The standard deviations of lithium concentration values calculated during rest periods, during which no current was applied, of each GITT test were determined and averaged. The average standard deviation during a rest period, i.e. the minimum detection limit, was 0.002 mol l^{-1}. This value represents the precision of the method. The establishment of a relationship between absorbance ratio and lithium concentration, as opposed to relying only on the lithium-shifted IR bands, automatically corrects for changes in penetration depth and electrode porosity. The signal strength, manifested as IR band height, can be affected by the level of wetting and amount of liquid in the IR path, e.g. porosity. Because the lithium concentration measurement is based on the heights of two distinct bands that will be equally affected by varying signal strengths, the ratio cancels out signal fluctuations not due to changes in lithium concentration. Thus, this correlation can be used for different battery sizes, configurations, and electrode structures.

The 1 C charging rate was achieved by applying a current of 300 μA to the half-cell (Fig. 5). The voltage response of decreasing potential during intercalation is typical of graphite half-cells. During charging, lithium ion concentration decreased rapidly by 1.5%. The changes in lithium concentration corresponded with increases in the magnitude of the current. The lithium concentration also relaxed after the current was turned off. Ideally, the lithium concentration in the anode would be nearly constant across its thickness. Lithium ions intercalating into the anode would be immediately replaced by the arrival of the new ions driven by concentration and charge polarization. The observed decrease in lithium concentration at the back of the anode represents a limitation of lithium ion transport across the electrolyte relative to the rate of intercalation into the graphite anode.

There is a slight delay between when the current is turned on and when the IR spectra begin to change. The delay is approximately 18 s, while the temporal resolution of the FTIR measurement is 25 s, so this delay could be partly due to temporal resolution limits. Additionally, the shape of the spectral response followed a square root of time form, especially in Fig. 6, which indicated that a diffusion controlled process was measured.

The 2.33 C charging rate was achieved by applying a current of 700 μA to the half-cell (Fig. 6). During the 2.33 C discharge, the lithium concentration increased by 2% on average across a distance of 2 μm, the penetration depth, from the electrode surface. The penetration depth was calculated using Eq. 2

$$d_p = \frac{\lambda}{2\pi n_1 \sqrt{\sin^2\theta - \left(\frac{n_2}{n_1}\right)^2}} \quad [2]$$

where d_p is the penetration depth in μm, λ is the wavelength in μm, n_1 is the refractive index of the ATR crystal (diamond), θ is the angle of incidence, and n_2 is the refractive index of the sample.[41] The refractive index of the electrolyte-soaked anode was calculated using Eq. 3

$$n_2 = n_{anode}*(1 - \phi) + (n_{electrolyte}*\phi) \quad [3]$$

where n_{anode} was determined by calculating a weighted average of the refractive indexes of the anode components: graphite, carbon black, and PVDF binder;[42–44] $n_{electrolyte}$ was determined by averaging the refractive indexes of EMC and EC;[45,46] and ϕ is the porosity of the anode. The porosity of the anode was not known, so a

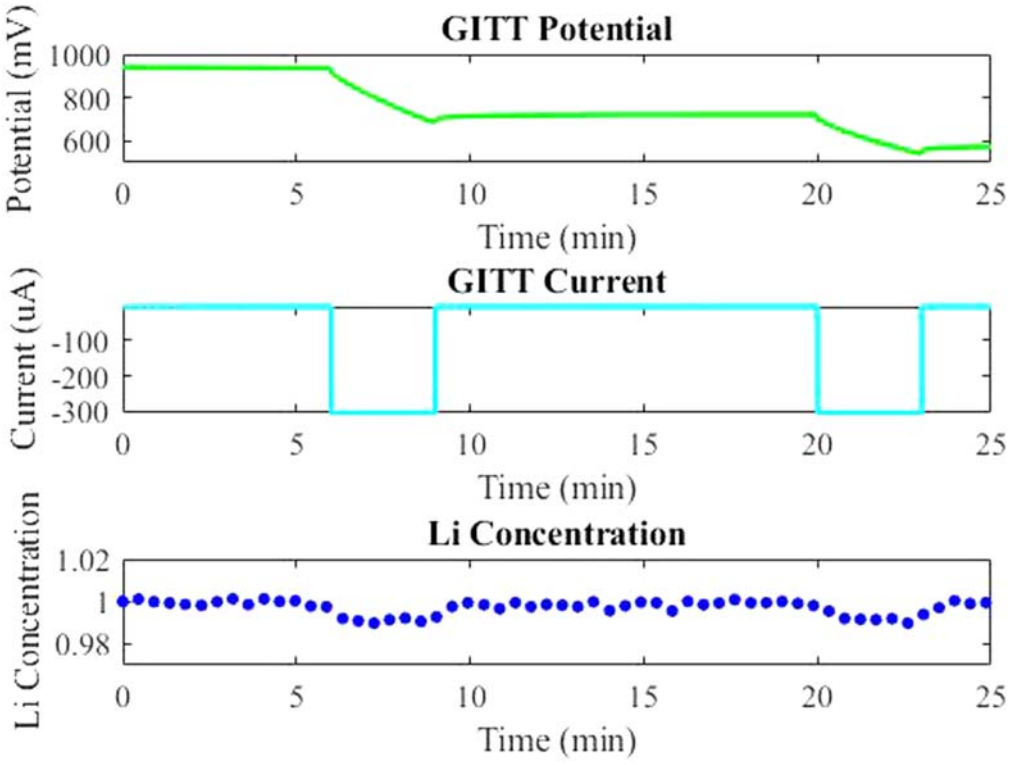

Figure 5. Operating potential and current during intercalation at 1 C/300 μA. Lithium concentration has been normalized to initial value.

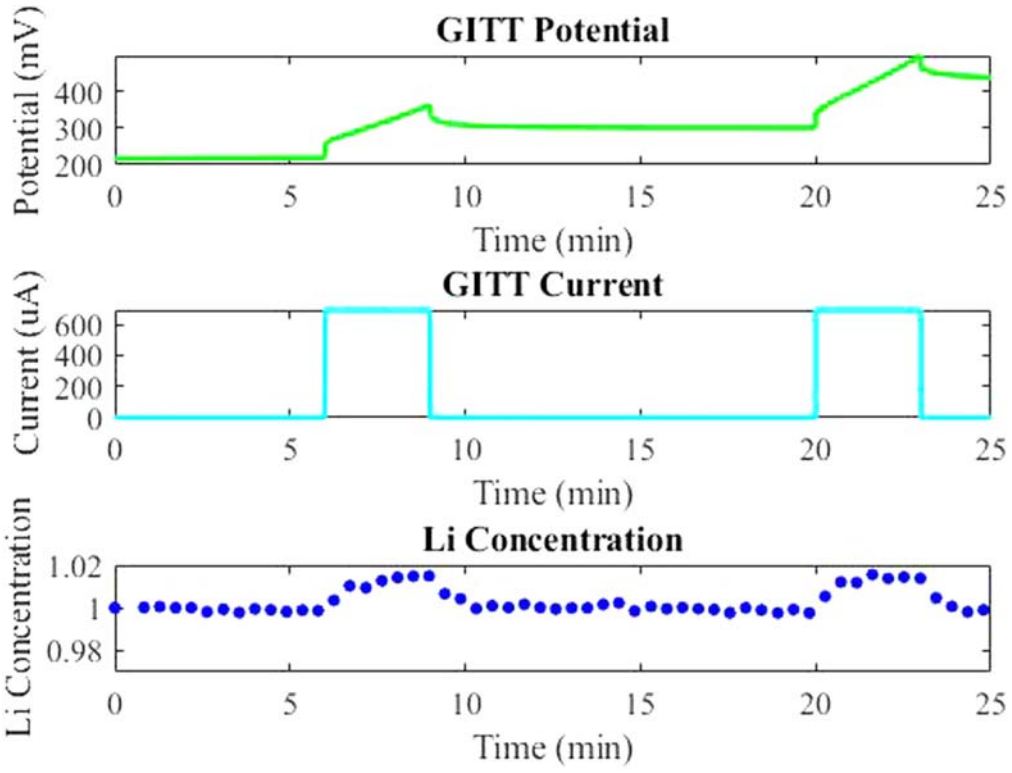

Figure 6. Operating potential and current during deintercalation at 2.33 C/700 μA. Lithium concentration has been normalized to initial value.

porosity value of 40% was selected from literature and used to determine the refractive index of the anode.[47] The refractive index of diamond is 2.42.[48] The angle of incidence is 45°, according to the Pike GladiATR™ manual.

Discharging (deintercalation) at 2.33 C caused the lithium ion concentration to increase because the rate of lithium ion deintercalation exceeded the transport rate in the electrolyte. The magnitude of the change in the lithium concentration was about 42% greater in the

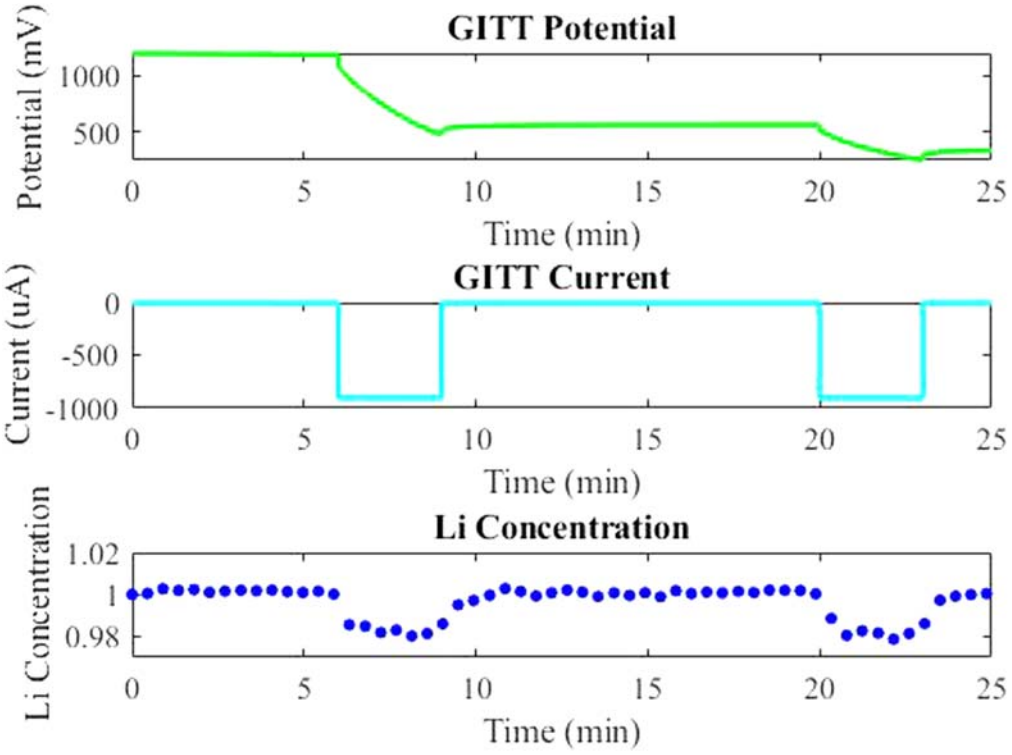

Figure 7. Operating potential and current during intercalation at 3 C/900 μA. Lithium concentration has been normalized to initial value.

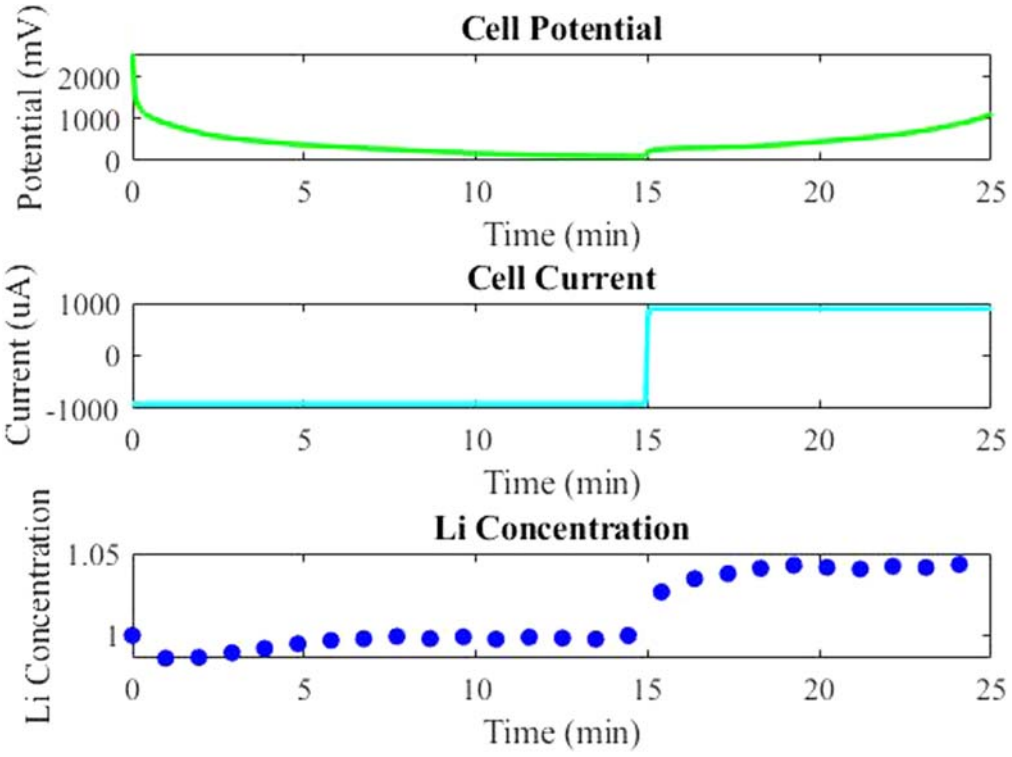

Figure 8. Operating potential and current during intercalation during 3 C/900 μA cycle. Lithium concentration has been normalized to initial value.

2.33 C case, compared to the 1 C case, reflecting the increased charging demand placed on the cell.

The 3 C charging rate was achieved by applying a current of 900 μA to the half-cell (Fig. 7). During the 3 C charge, the lithium concentration decreased rapidly by 2.4%. Similarly to the 1 C case, decreased lithium concentration corresponded with current increases, and lithium concentration also relaxed after current was turned off. Again, the greater charge demand placed on the cell was unable to be met by the transport capability of the electrolyte, so there were noticeable decreases in lithium concentration at the back

of the anode, and those decreases in concentration were directly related to the magnitude of the current applied to the cell. The location of lithium concentration measurement was at the back of the anode, the side of the anode closest to the ATR plate. This position likely corresponded with the largest deviations in ion concentration because this location was the furthest point from the lithium electrode. A recent model of a graphite anode in a Li-ion battery also estimated the lithium depletion phenomenon.[34] The results of this research did not show the magnitude of lithium concentration decreases calculated by Colclasure et al. For example, at a C-rate of 1C, Colclasure et al. estimated a variation of 17% in a graphite electrode. This variation is likely a result of the modeled system being a full cell with thicker electrodes (47 μm vs 20 μm). In general, the correlation of increased C-rates with increased lithium concentration variation did match that of the model.

The lithium concentration change during a non-GITT cycle is also an important metric for battery performance. A 3C cycle, shown in Fig. 8, was conducted on the same Li-ion half-cell and consisted of a constant current of -900 μA being applied until the cell reached 150 mV at which point a positive current was applied. As expected, the lithium ion concentration increased abruptly as the current was reversed, which indicates rapid deintercalation. The lithium ion concentration at the back of the anode changed by over 5% during cycling. This finding motivates further study at higher C-rates during which greater depletion is likely to occur. Lastly, in a test with 10 consecutive 6C cycles, we did not observe an overall lithium depletion between the beginning of the 10-cycle test and the end.

Conclusions and Discussion

IR spectral solvation shifting was utilized to develop a quantitative diagnostic of lithium concentration suitable for operando measurements of liquid battery electrolytes. The diagnostic was demonstrated by operando FTIR/ATR measurements at a collection rate of 2 measurements per minute on a lithium metal-graphite anode half-cell using intermittent charging/discharging. Local lithium ion depletion and accumulation due to insufficient ion transport were observed to increase at higher charge and discharge rates, respectively. The movement of lithium is the critical aspect of the function of Li-ion batteries, as well as a limiting factor for improving battery performance. The newfound capability to quantitatively observe lithium concentrations in real time has significant promise for battery performance analysis, especially under fast-charging conditions. This operando observation technique should prove especially suitable for the study of EV batteries with thicker electrodes, as thicker electrodes will experience greater electrolyte lithium ion depletion within the anode.

ORCID

Lydia Meyer https://orcid.org/0000-0002-2361-1512

References

1. J. Tarascon and M. Armand, "Issues and Challenges Facing Rechargeable Lithium Batteries." *Nature*, **414**, 359 (2001).
2. M. Armand and J.-M. Tarascon, "Building Better Batteries." *Nature*, **451**, 652 (2008).
3. Y. Liu, Y. Zhu, and Y. Cui, "Challenges and opportunities towards fast-charging battery materials." *Nat. Energy*, **4**, 540 (2019).
4. M. Keyser et al., "Enabling fast charging - Battery thermal considerations." *Journal of Power Sources*, **367**, 228 (2017).
5. A. Hoke, A. Brissette, K. Smith, A. Pratt, and D. Maksimovic, "Accounting for Lithium-Ion Battery Degradation in Electric Vehicle Charging Optimization." *IEEE J. Emerg. Sel. Top. Power Electron.*, **2**, 691 (2014).
6. S. Ahmed et al., "Enabling fast charging - A battery technology gap assessment." *Journal of Power Sources*, **367**, 250 (2017).
7. K. M. Diederichsen, E. J. McShane, and B. D. McCloskey, "Promising Routes to a High Li+ Transference Number Electrolyte for Lithium Ion Batteries." *ACS Energy Lett.*, **2**, 2563 (2017).
8. M. R. Palacín and A. d. Guibert, "Why do batteries fail?" *Science*, **351** (2016).
9. G. Gachot, S. Grugeon, M. Armand, S. Pilard, P. Guenot, J.-M. Tarascon, and S. Laruelle, "Deciphering the multi-step degradation mechanisms of carbonate-based electrolyte in Li batteries." *Journal of Power Sources*, **178**, 409 (2008).
10. F. Shi, H. Zhao, G. Liu, P. N. Ross, G. A. Somorjai, and K. Komvopoulos, "Identification of Diethyl 2,5-Dioxahexane Dicarboxylate and Polyethylene Carbonate as Decomposition Products of Ethylene Carbonate Based Electrolytes by Fourier Transform Infrared Spectroscopy." *The Journal of Physical Chemistry C*, **118**, 14732 (2014).
11. K. Hongyou, T. Hattori, Y. Nagai, T. Tanaka, H. Nii, and K. Shoda, "Dynamic in situ fourier transform infrared measurements of chemical bonds of electrolyte solvents during the initial charging process in a Li ion battery." *Journal of Power Sources*, **243**, 72 (2013).
12. T. Zhang, B. Fuchs, M. Secchiaroli, M. Wohlfahrt-Mehrens, and S. Dsoke, "Electrochemical behavior and stability of a commercial activated carbon in various organic electrolyte combinations containing Li-salts." *Electrochimica Acta*, **218**, 163 (2016).
13. L. Yang, B. Ravdel, and B. L. Lucht, "Electrolyte Reactions with the Surface of High Voltage LiNi0.5Mn1.5O4 Cathodes for Lithium-Ion Batteries." *Electrochem. Solid-State Lett.*, **13**, A95 (2010).
14. J. Yang, N. Solomatin, A. Kraytsberg, and Y. Ein-Eli, "In-Situ Spectro-electrochemical Insight Revealing Distinctive Silicon Anode Solid Electrolyte Interphase Formation in a Lithium-ion Battery." *ChemistrySelect*, **1**, 572 (2016).
15. S. F. Lux, M. Schmuck, S. Jeong, S. Passerini, M. Winter, and A. Balducci, "Li-ion anodes in air-stable and hydrophobic ionic liquid-based electrolyte for safer and greener batteries." *International Journal of Energy Research*, **34**, 97 (2010).
16. M. Moshkovich, M. Cojocaru, H. E. Gottlieb, and D. Aurbach, "The study of the anodic stability of alkyl carbonate solutions by in situ FTIR spectroscopy, EQCM, NMR and MS,." *Journal of Electroanalytical Chemistry*, **497**, 84 (2001).
17. C. M. Burba and R. Frech, "In situ transmission FTIR spectroelectrochemistry: A new technique for studying lithium batteries." *Electrochimica Acta*, **52**, 780 (2006).
18. J.-T. Li, S.-R. Chen, F.-S. Ke, G.-Z. Wei, L. Huang, and S.-G. Sun, "In situ microscope FTIR spectroscopic studies of interfacial reactions of Sn-Co alloy film anode of lithium ion battery." *Journal of Electroanalytical Chemistry*, **649**, 171 (2010).
19. X. Chen, X.-Q. Zhang, H.-R. Li, and Q. Zhang, "Cation-Solvent, Cation-Anion, and Solvent-Solvent Interactions with Electrolyte Solvation in Lithium Batteries." *Batteries & Supercaps*, **2**, 128 (2019).
20. O. Borodin, M. Olguin, P. Ganesh, P. R. C. Kent, J. L. Allen, and W. A. Henderson, "Competitive lithium solvation of linear and cyclic carbonates from quantum chemistry." *Phys. Chem. Chem. Phys.*, **18**, 164 (2016).
21. K. Xu, "Charge-Transfer Process at Graphite/Electrolyte Interface and the Solvation Sheath Structure of Li[sup +] in Nonaqueous Electrolytes." *J. Electrochem. Soc.*, **154**, A162 (2007).
22. K. Xu, Y. Lam, S. S. Zhang, T. R. Jow, and T. B. Curtis, "Solvation Sheath of Li+ in Nonaqueous Electrolytes and Its Implication of Graphite/Electrolyte Interface Chemistry." *The Journal of Physical Chemistry C*, **111**, 7411 (2007).
23. L. Yang, A. Xiao, and B. L. Lucht, "Investigation of solvation in lithium ion battery electrolytes by NMR spectroscopy." *Journal of Molecular Liquids*, **154**, 131 (2010).
24. K. Matsubara, R. Kaneuchi, and N. Maekita, "13 C NMR estimation of preferential solvation of lithium ions in non-aqueous mixed solvents," Journal of The Chemical Society." *Faraday Transactions*, **94**, 3601 (1998).
25. S. A. Krachkovskiy, J. D. Bazak, P. Werhun, B. J. Balcom, I. C. Halalay, and G. R. Goward, "Visualization of Steady-State Ionic Concentration Profiles Formed in Electrolytes during Li-Ion Battery Operation and Determination of Mass-Transport Properties by in Situ Magnetic Resonance Imaging." *J. Am. Chem. Soc.*, **138**, 7992 (2016).
26. S. A. Krachkovskiy, J. M. Foster, J. D. Bazak, B. J. Balcom, and G. R. Goward, "Operando Mapping of Li Concentration Profiles and Phase Transformations in Graphite Electrodes by Magnetic Resonance Imaging and Nuclear Magnetic Resonance Spectroscopy." *Journal of Physical Chemistry C*, **122**, 21784 (2018).
27. T. Tanim, P. Paul, V. Thampy, C. Cao, H. Steinruck, J. Nelson Weker, M. Toney, E. Dufek, M. Evans, A. Jansen, B. Polzin, A. Dunlop, and S. Trask, "Heterogeneous Behavior of Lithium Plating during Extreme Fast Charging." *Cell Reports Physical Science*, **1**, 100114 (2020).
28. K. D. Fulfer and D. G. Kuroda, "A comparison of the solvation structure and dynamics of the lithium ion in linear organic carbonates with different alkyl chain lengths." *Phys. Chem. Chem. Phys.*, **19**, 25140 (2017).
29. K. D. Fulfer and D. G. Kuroda, "Solvation Structure and Dynamics of the Lithium Ion in Organic Carbonate-Based Electrolytes: A Time-Dependent Infrared Spectroscopy Study." *The Journal of Physical Chemistry C*, **120**, 24011 (2016).
30. T. Yamanaka, H. Nakagawa, S. Tsubouchi, Y. Domi, T. Doi, T. Abe, and Z. Ogumi, "In situ diagnosis of the electrolyte solution in a laminate lithium ion battery by using ultrafine multi-probe Raman spectroscopy." *Journal of Power Sources*, **359**, 435 (2017).
31. C. Marino, A. Boulaoued, J. Fullenwarth, D. Maurin, N. Louvain, J. Bantignies, L. Stievano, and L. Monconduit, "Solvation and Dynamics of Lithium Ions in Carbonate-Based Electrolytes during Cycling Followed by Operando Infrared Spectroscopy: The Example of NiSb2, a Typical Negative Conversion-Type Electrode Material for Lithium Batteries." *The Journal of Physical Chemistry C*, **121**, 26598 (2017).
32. L. D. Ellis, S. Buteau, S. G. Hames, L. M. Thompson, D. S. Hall, and J. R. Dahn, "A New Method for Determining the Concentration of Electrolyte Components in

Lithium-Ion Cells, Using Fourier Transform Infrared Spectroscopy and Machine Learning." *J. Electrochem. Soc.*, **165**, A256 (2018).
33. P. P. Paul et al., "A Review of Existing and Emerging Methods for Lithium Detection and Characterization in Li-Ion and Li-Metal Batteries." *Adv. Energy Mater.*, **11**, 2100372 (2021).
34. A. M. Colclasure et al., "Electrode scale and electrolyte transport effects on extreme fast charging of lithium-ion cells." *Electrochimica Acta*, **337**, 135854 (2020).
35. A. Verma, K. Smith, S. Santhanagopalan, D. Abraham, K. P. Yao, and P. P. Mukherjee, "Galvanostatic Intermittent Titration and Performance Based Analysis of LiNi0.5Co0.2Mn0.3O2 Cathode." *J. Electrochem. Soc.*, **164**, A3380 (2017).
36. L. D. Kock, M. D. S. Lekgoathi, P. L. Crouse, and B. M. Vilakazi, "Solid state vibrational spectroscopy of anhydrous lithium hexafluorophosphate (LiPF6)." *Journal of Molecular Structure*, **1026**, 145 (2012).
37. M. Masia, M. Probst, and R. Rey, "Ethylene Carbonate-Li.: A Theoretical Study of Structural and Vibrational Properties in Gas and Liquid Phases." *The Journal of Physical Chemistry B*, **108**, 2016 (2004).
38. R. Aroca, M. Nazri, G. A. Nazri, A. J. Camargo, and M. Trsic, "Vibrational Spectra and Ion-Pair Properties of Lithium Hexafluorophosphate in Ethylene Carbonate Based Mixed-Solvent Systems for Lithium Batteries." *Journal of Solution Chemistry*, **29**, 1047 (2000).
39. M. Matsui, S. Deguchi, H. Kuwata, and N. Imanishi, "In-operando FTIR Spectroscopy for Composite Electrodes of Lithium-ion Batteries." *Electrochemistry*, **83**, 874 (2015).
40. M. D. Bhatt and C. O'Dwyer, "Density functional theory calculations for ethylene carbonate-based binary electrolyte mixtures in lithium ion batteries." *Curr. Appl. Phys.*, **14**, 349 (2014).
41. J. Grdadolnik, "ATR-FTIR Spectroscopy: Its Advantages and Limitations." *Acta Chim. Slov.*, **49**, 13 (2002).
42. A. B. Djurišić and E. H. Li, "Optical properties of graphite." *J. Appl. Phys.*, **85**, 7404 (1999).
43. A. P. Indolia and M. S. Gaur, "Optical properties of solution grown PVDF-ZnO nanocomposite thin films." *Journal of Polymer Research*, **20**, 43 (2012).
44. F. Liu, J. Yon, A. Fuentes, P. Lobo, G. J. Smallwood, and J. C. Corbin, "Review of recent literature on the light absorption properties of black carbon: Refractive index, mass absorption cross section, and absorption function." *Aerosol Science and Technology*, **54**, 33 (2020).
45. D. R. Lide, *CRC Handbook of Chemistry and Physics* (CRC Press, Boca Raton, FL) 85th ed. (2004).
46. P. Škubla and W. Waradzin, "Kinematic viscosities of acetone, vinyl acetate, crotonaldehyde, acetic acid, acetic anhydride and their binary and ternary mixtures." *Collection of Czechoslovak Chemical Communications*, **48**, 3508 (1983).
47. P. Novák, W. Scheifele, M. Winter, and O. Haas, "Graphite electrodes with tailored porosity for rechargeable ion-transfer batteries." *Journal of Power Sources*, **68**, 267 (1997).
48. H. R. Phillip and E. A. Taft, "Kramers-Kronig Analysis of Reflectance Data for Diamond." *Phys. Rev.*, **136**, A1445 (1964).